Supporting Information

Insight into multivalent iron complex-bound oxygen vacancy-rich BiOBr nanodiscs for photocatalytic ammonia synthesis

Vinay Kumar Sriramadasu[a],† Himani Joshi[b],† Ibamerisha Lyngdoh[a], Naveen Sharma[b], Srimanta Pakhira [b, c]* and Santanu Bhattacharyya [a] *

[a] Department of Chemical Sciences, Indian Institute of Science Education and Research (IISER) Berhampur, Berhampur-760010, Odisha, India.

[b] *Theoretical Condensed Matter Physics and Advanced Computational Materials Science Laboratory*, Department of Physics, Indian Institute of Technology Indore, Simrol, Khandwa Road, Indore, Madhya Pradesh, 453552, India.

[c] *Theoretical Condensed Matter Physics and Advanced Computational Materials Science Laboratory*, Centre for Advanced Electronics (CAE), Indian Institute of Technology Indore, Simrol, Khandwa Road, Indore, Madhya Pradesh, 453552, India.

*Corresponding Author's Emails: *-santanub@iiserbpr.ac.in (S.B.)

spakhira@iiti.ac.in or spakhirafsu@gmail.com (S.P.)

†Mr. Vinay Kumar Sriramadasu and Ms. Himani Joshi contributed equally to this manuscript.

Experimental Section

Chemical requirement

Bismuth (III) nitrate pentahydrate [$Bi(NO_3)_3.5H_2O$], potassium bromide [KBr], Ferric (III) nitrate nonahydrate [$Fe(NO_3)_3.9H_2O$], phytic acid (PA) [$C_6H_{18}O_{24}P_6$], sodium hydroxide [NaOH], ethylene glycol (EG) [$(CH_2OH)_2$], ammonium chloride [NH_4Cl], dextrose [$C_6H_{12}O_6$], salicylic acid [$C_7H_6O_3$], sodium hypo chlorate [NaClO], sodium nitroferricyanide [$Na_2[Fe(CN)_5NO]_2.H_2O$], hydrazine hydrate [$N_2H_4.H_2O$], sulfuric acid [H_2SO_4], para-(dimethylamino) benzaldehyde [$C_9H_{11}NO$], Acetonitrile (ACN) [C_2H_3N], hydrochloric acid [HCl], sodium sulfate [Na_2SO_4] were obtained from Loba Chemical Pvt. Ltd.(India). Methanol (CH_3OH), sodium citrate [$C_6H_5Na_3O_7$], and ethanol (C_2H_5OH) were purchased from Sigma-Aldrich. All the chemicals are analytical grade and are used directly without further purification. Double-distilled water (DDW) was used throughout the experiments.

Preparation of photocatalysts

Synthesis of Fe-Phytic acid complex (Fe-PA) powder

The metal-PA complex has been prepared in an ethanol solution at room temperature. A 3 mmol. of $Fe(NO_3)_3.9H_2O$ is added into EtOH (30 mL) and kept under stirring for 30 min to dissolve it completely. PA of 0.5 mmol (molar ratio of PA: Fe = 1:6) is added to the above-prepared Fe-solution under stirring conditions. The stirring is continued for 12 h to achieve the complex of iron and PA. Afterward, the precipitate was collected and washed with water and ethanol through the centrifugation process. The obtained material was dried and named as Fe-PA.

Synthesis of $BiOBr_{OV}@Fe_x$, $BiOBr_{OV,}$ and BiOBr

2 mmol of $Bi(NO_3)_3.5H_2O$ has been dissolved in 10 mL of EG under stirring conditions. Various weights of early prepared Fe-PA powder (x = 2, 3, 5, 7.5, 10 mg) were added to the prepared $Bi(NO_3)_3$ solution. The homogeneous dispersion is achieved by bath sonication and stirring. Afterward, 10 mL of aqueous solution containing 2 mmol KBr was added dropwise into the above-prepared solution, and the stirring condition was continued for another 30 min. The whole mixture was transferred to the autoclaves for the solvothermal reaction at 180 ^oC

for 18 h. After completion of the reaction, the obtained precipitate was washed through the centrifugation process with water & ethanol. The material was dried overnight and named as $BOB_{OV}@Fe_x$, whereas 'x' represents the amount of Fe-PA powder utilized in the reaction.

The oxygen vacancies-rich BiOBr, i.e., BOB_{OV}, has been prepared by following the same procedure, without the addition of the Fe-PA powder.

The oxygen defect-free BiOBr (BOB) has been synthesized by calcinating the BOB_{OV} in an open-air atmosphere at 350 ^{O}C for 4 h.

Synthesis of $BiOBr_{OV}@Ni_5$, $BiOBr_{OV}@C$, $BiOBr_{OV}@PA$

Under the same synthesis process of $BOB_{OV}@Fe_5$, $BOB_{OV}@C$, $BOB_{OV}@PA$, and $BOB_{OV}@Ni_5$ are prepared by using a reasonable amount of glucose (22 mg), phytic acid (1 mmol), and Ni-Phytic acid complex powder (5 mg), respectively.

Characterization

Structural morphological properties are examined by A Joel-made JSM-7610F Field Emission Scanning Electron Microscope (FESEM). A high-resolution transmission electron microscope (HR-TEM), Joel JEM-2100 Plus, was employed to record TEM and HR-TEM images, energy dispersive x-ray spectroscopy spectra (EDS), and selected area electron diffraction (SAED) patterns. The X-ray photoelectron spectroscopy (XPS) instrument of the PHI 5000 Versa Probe-II has been used to analyze the chemical states of as-synthesized materials. XRD patterns are recorded using an X-ray diffractometer (XRD), Empyrean model, PANalytical. B.V. BELSORP MAX II, MICROTRAC-MRB was utilized to perform N_2 adsorption-desorption studies to reveal the surface area and pore details. A Cary 5000, an Agilent spectrophotometer, has been utilized to record both UV-vis. diffusion reflectance spectra of the material and absorption spectra of the reaction liquor. Photoluminescence (PL) properties were carried out on a Horiba-made Fluorolog-3 spectrofluorometer. Time-resolved PL spectra have been recorded by using the TCSPC setup of Lifespec-II of Edinburgh. Oxygen vacancies were identified by electron paramagnetic resonance (EPR) spectroscopy of JES FA200, Joel. ^{1}H nuclear magnetic resonance (NMR) spectra were recorded at 400 MHz FT-NMR in DMSO–d6 solvent by Bruker-made AVANCE NEO Ascend 400. A high-resolution mass spectrometer (HRMS), Xevo G2-XS QT of a Quadrupole Time of Flight Mass Spectrometer, Waters, has been utilized for the HRMS data.

Photo-Electrochemical Measurements

The (photo) electrochemical studies have been done by using A CHI-760E electrochemical workstation (CH Instruments, USA) with an external portable Xenon light source, an Ashai-made MAX-350 with a bandpass filter (380 – 700 nm). The three-electrode configuration is used as the experimental setup with 0.1 M Na_2SO_4 aqueous solution as an electrolyte. The drop-casted material on FTO-coated glass substrate, Ag/AgCl electrode, and Pt wire electrodes are utilized as the working electrode, reference electrode, and counter electrode, respectively. To fabricate the working electrode, 1 mg of the material was added to 1 mL of ethanol and sonicated for proper dispersion. 10 µL of Nafion solution was mixed into the mixture, which is used as a binder. The prepared slurry was cast in the lower area of 1 x 1 cm^2 of FTO glass and dried to evaporate the solution. Techniques employed: (i) AC Impedance (IMP) having frequency: 0.1 – 1 $x10^6$ Hz & Open circuit potential value for E, (ii) Impedance – Potential (IMPE) with E = ± 2 V & 1 kHz, and (iii) Amperometric I-t curve with E = 0.1 V.

Photocatalytic N_2 reduction reaction

All the prepared photocatalysts were evaluated for photocatalytic ammonia production in a sealed quartz container under a customized LED-based light source, at room temperature. The customized light source is made by circularly coiling the commercially available 35 W LED strip (cool white color, 120 no s LEDs, 5 meters) inside a hollow wooden cylinder (1 foot diameter). For comparison, a 300 W Xe light source (Newport, USA) was used. For the reaction, the prepared reaction mixture is sealed in a quartz container, and it is kept at the center of the wooden box where all the LEDs' light converges.

Typically, 10 mg of photocatalyst is suspended in 10 mL of aqueous methanol (1 v/v%) and sealed with a rubber septum.[1] The N_2 gas from the cylinder has been passed through 1 M H_2SO_4 and pure water to eliminate the gaseous impurities in it, before purging into the container. The N_2 gas was bubbled for 30 min to get an equilibrium of the N_2 atmosphere inside the container. Afterward, the homogeneous dispersed mixture was illuminated under the light source for 2 h to check the photocatalytic activity for NRR. After completion of the reaction, the filtered aliquot was taken for the Indophenol test to quantify the produced ammonia.[2,3] To reveal the critical roles of H_2O and N_2 gas, the reaction was conducted in acetonitrile solvent

and a saturated Ar atmosphere, respectively.[4,5] The formation of an intermediate product, i.e., N_2H_4, was examined by the Watts & Chrisp method.[2] The stability of the material for photocatalysis was evaluated for 5 cycles. For that, after completion of the 1st reaction, the used photocatalyst material was collected by centrifugation, and it was used for the next consecutive (i.e., 2nd) reaction, and so on. The wavelength-dependent photocatalytic activity for NRR is examined by using the various filters (380, 400, 420, 450 nm, ±5 nm) in the Ashai MAX-350, an Xe-based light source. From the obtained production data, the apparent quantum yield (AQY) of the photocatalyst for the NH_3 production has been calculated by using the equation,

$$AQY(\%) = \frac{produced\ NH_3\ (mol)\ X\ 6}{No.\ of\ Photon\ used\ \ X\ 100} \quad \text{....Equation S1}$$

Theory and Computational Details

A BiOBr monolayer was computationally designed by cleaving the (001) plane of pristine bulk BiOBr (P4/nmm space group). A 3×3×1 supercell of the BiOBr monolayer was subsequently modelled following the structural framework established in previous studies.[6] To eliminate artificial interactions between periodic images in a calculation, a vacuum space of 15 Å was introduced along the z-direction. Subsequently, an oxygen vacancy was created to model the BOB_{OV} monolayer, and Fe doping was introduced in this oxygen vacant BOB_{OV} by replacing one Bi atom adjacent to the oxygen vacant site to model the $BOB_{OV}@Fe_x$ monolayer (**Figure 4a-d**). We utilized the first principles-based Vienna *Ab Initio* Simulation Package (VASP) suite code to obtain all the relaxed equilibrium geometries (BOB, BOB_{OV}, $BOB_{OV}@Fe_x$, and intermediates formed during NRR) and to attain the adsorption free energy of all reaction intermediates by single-point calculations.[7,8] We have used the projector augmented wave (PAW) method to describe the interaction between the valence and core electrons of the system.[9] PBE (Perdew–Burke–Ernzerhof) functionals are utilized for geometry optimization and free energy calculations.[10] For the expansion of electronic wave functions, a plane wave cutoff energy of 520 eV, and ionic forces convergence criteria are set to -0.01 eV/ Å. For sampling of the Brillouin zone in k-space, we have used a Gamma-centred k-point grid of 2x2x1.

For electronic properties calculations such as band structures, density of states, and partial density of states of BOB, BOB_{OV}, and $BOB_{OV}@Fe_x$, we employed the first-principles hybrid functional-based B3LYP-D3 DFT method implemented in the CRYSTAL23 suite

code.[11] To eliminate artificial interactions between periodic images in a calculation, a vacuum space of 500 Å was introduced here along the z-direction by following the CRYSTAL23 suite code with an appropriate keyword. The B3LYP-D3 method is a more accurate and computationally feasible method for electronic property calculations and provides more reliable results in the case of electronic property studies in perovskite materials.[12] Further, Grimme's dispersion correction (-D3) for long-range interactions has been considered, i.e., the B3LYP-D3 method is utilized for all electronic property calculations.[13] In our present investigation, for the expansion of crystalline orbitals of the atoms Bi, Br, O, and Fe, we relied on a Gaussian basis set of triple-zeta valence with polarization quality (TZVP).[14] We identified a highly symmetric k-path $\Gamma - R - N - \Gamma$ in the first Brillouin zone, for the calculation of electronic bands. VESTA software was used to design and visualize all the designed structures.[15] For the calculation of the Gibbs free energy of formation of all the intermediates occurring during the reaction, we have used the following equation:[16]

$$\Delta G = \Delta E - \Delta E_{ZPE} - T\Delta S \qquad \text{.....Equation S2}$$

Here ΔG is the change in Gibbs free energy, ΔE is the adsorption energy (i.e., change of electronic energy computed by the DFT method), ΔE_{ZPE} is the change of zero-point vibrational energy and ΔS is the entropy correction term.

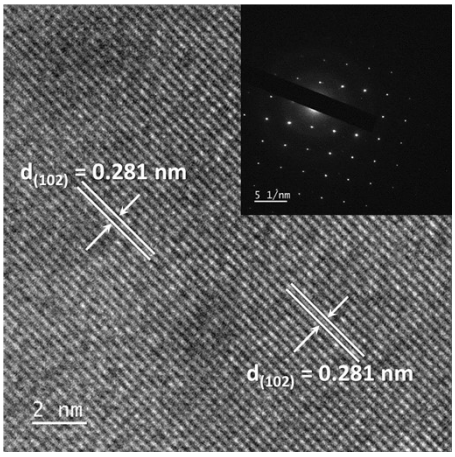

Figure S1. HR-TEM image (Inset image-SAED pattern) of BOB_{OV}.

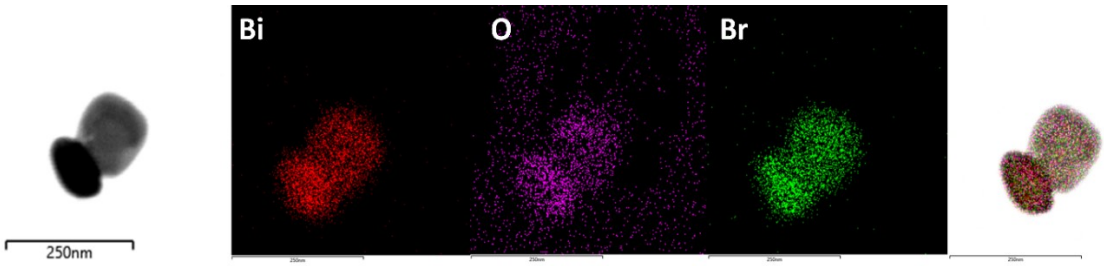

Figure S2. EDX elemental mapping of BOB_{OV}.

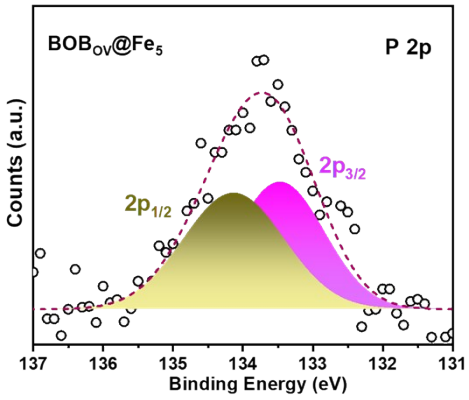

Figure S3. High-resolution XPS spectra of P 2p for $BOB_{OV}@Fe_5$.

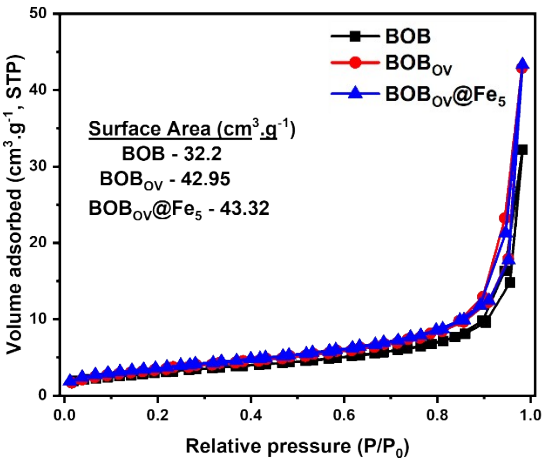

Figure S4. N_2 adsorption-desorption (BET) isotherms for BOB, BOB_{OV}, and $BOB_{OV}@Fe_5$.

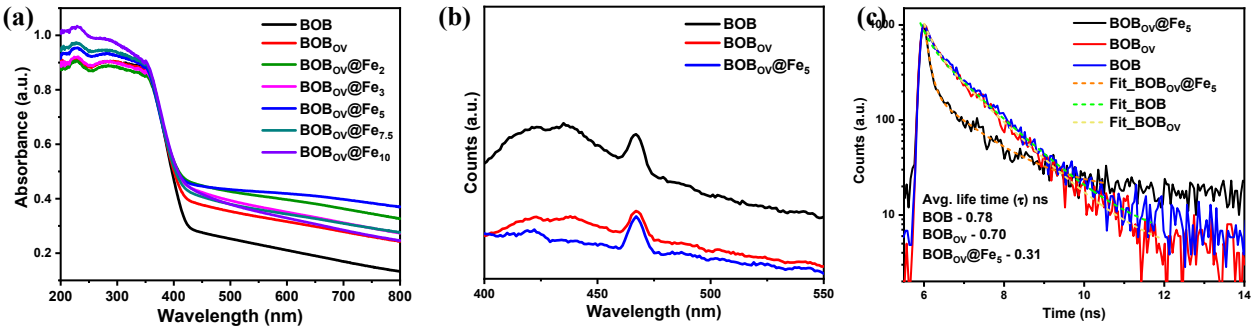

Figure S5. UV-vis DRS absorbance spectra of BOB, BOB_{OV}, and $BOB_{OV}@Fe_x$. Comparative (b) PL and (c) TRPL spectra of BOB, BOB_{OV}, and $BOB_{OV}@Fe_5$.

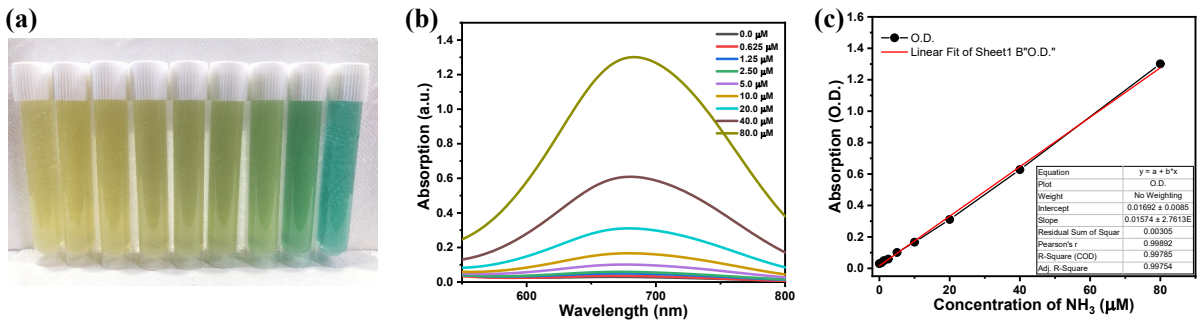

Figure S6. (a) A series of different known concentrations of ammonia solution with Indophenol reagent, (b) respective absorption spectra, and (c) A standard calibration curve plotted between the concentration of ammonia vs. their optical density values.

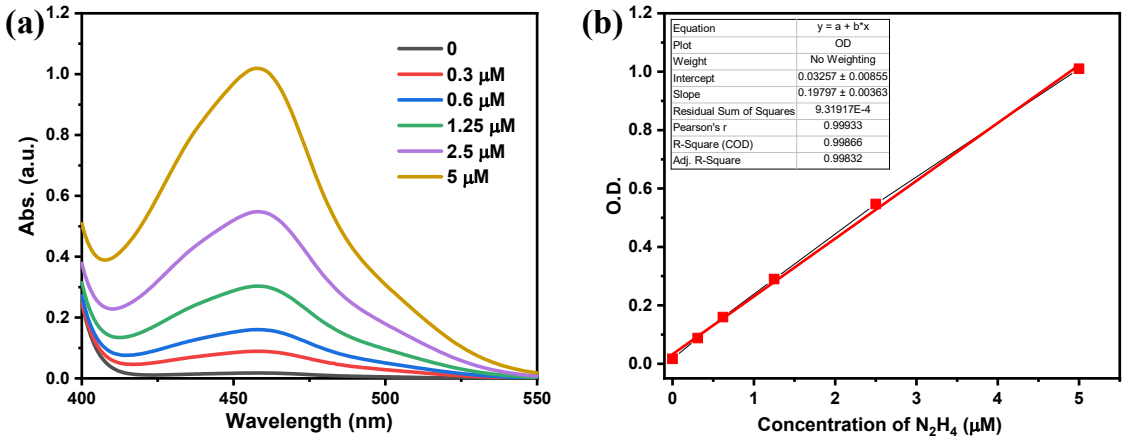

Figure S7. (a) Absorption spectra of known concentrations of N_2H_4, and (b) A standard calibration curve to quantify the formed N_2H_4.

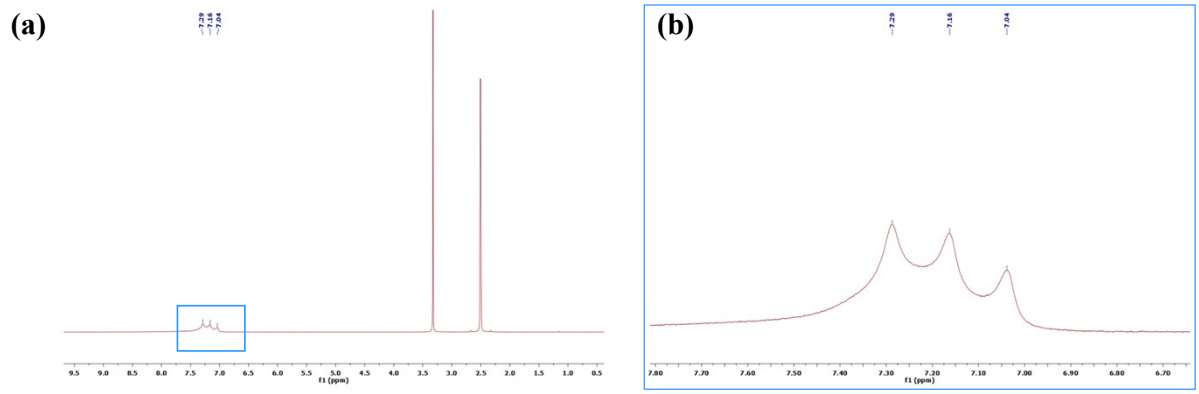

Figure S8. (a) 1H NMR spectra of the cumulative production of ammonia, (b) enlarged view of the peaks corresponding to the NH_4^+.

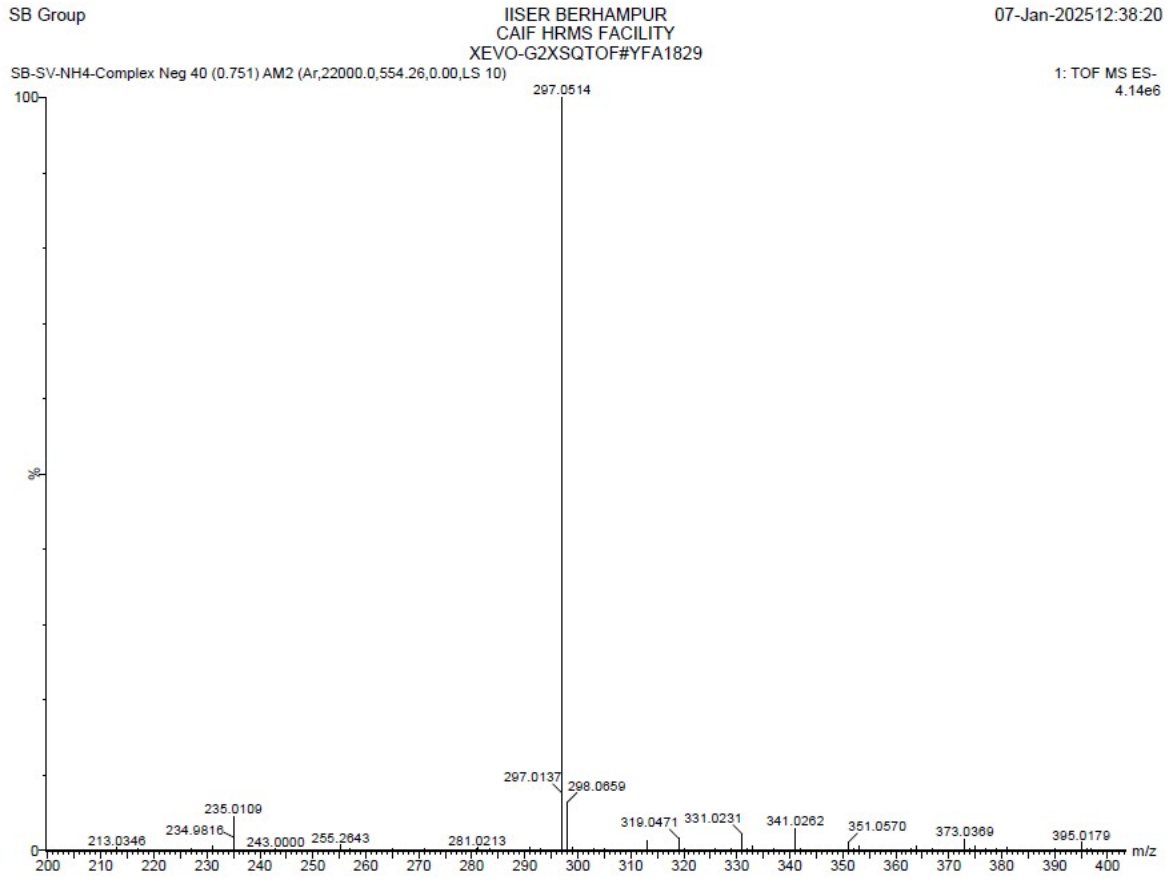

Figure S9. HR-MS data of the Indophenol complex formed by the photocatalytic produced ammonia.

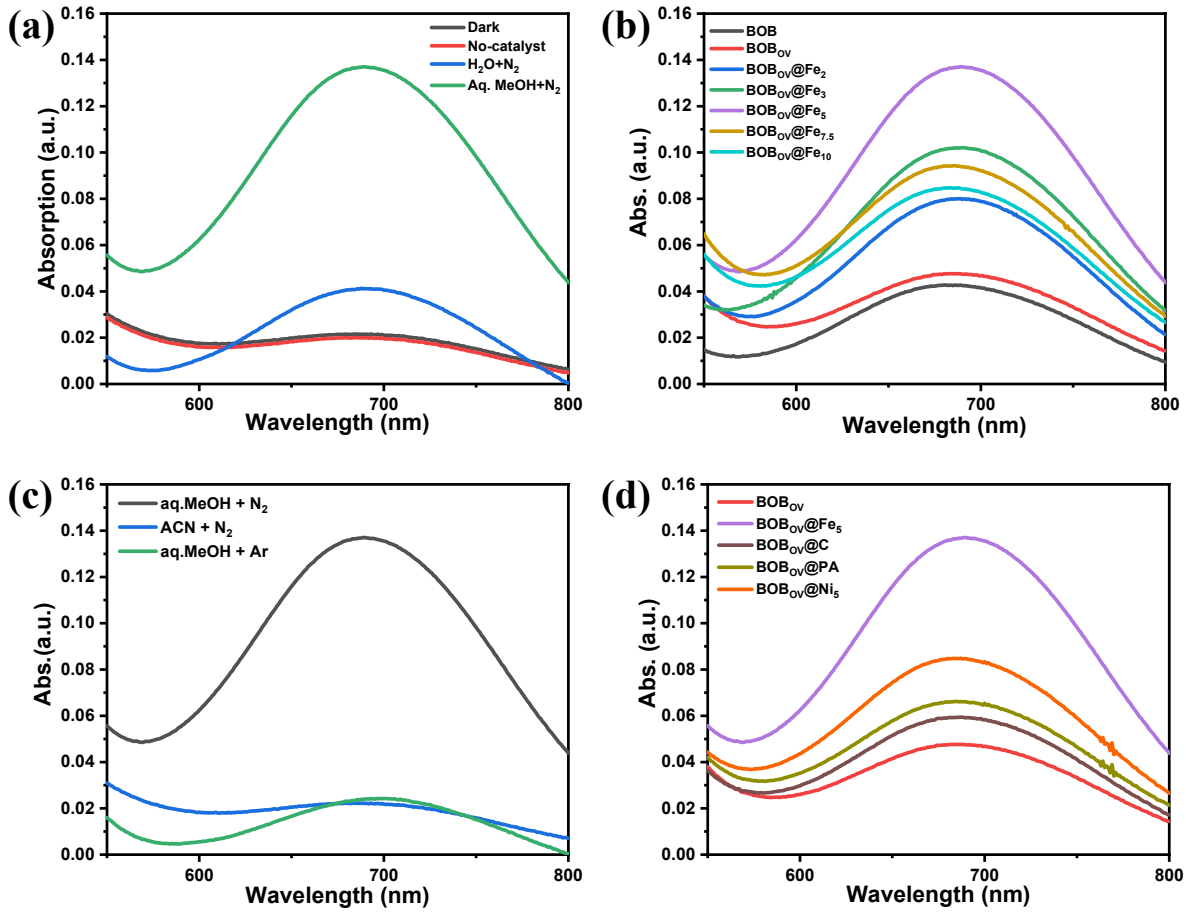

Figure S10. Absorption spectra of Indophenol tests for (a) photocatalytic reaction optimization, (b) different photocatalysts, (c) control experiments with Ar & ACN, and (d) control experiments for the active sites.

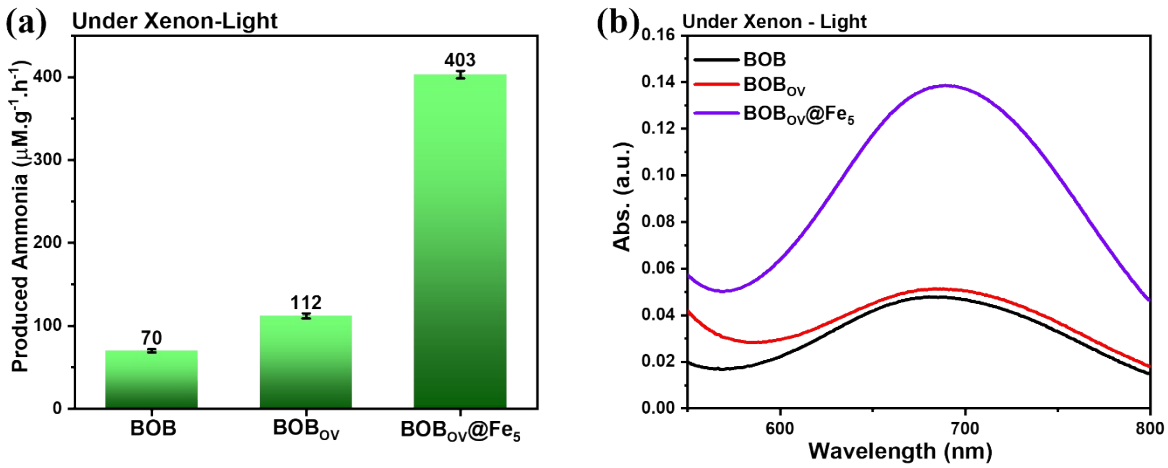

Figure S11. (a) Photocatalytic NH_3 production rates of BOB, BOB_{OV}, and $BOB_{OV}@Fe_5$ under a Xe light source, and (b) their respective absorption curves for the indophenol tests.

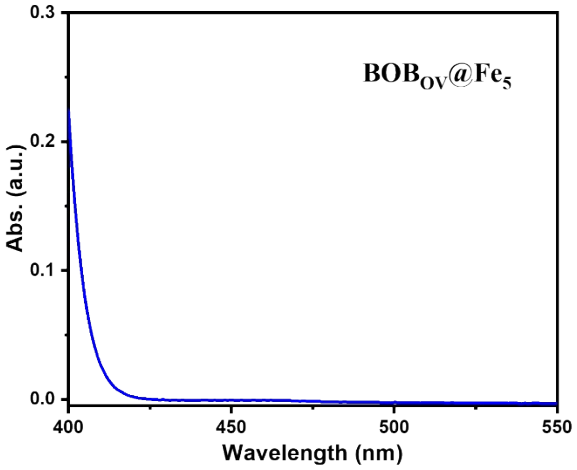

Figure S12. Absorption spectra of the Watt-Chrisp test for the $BOB_{OV}@Fe_5$.

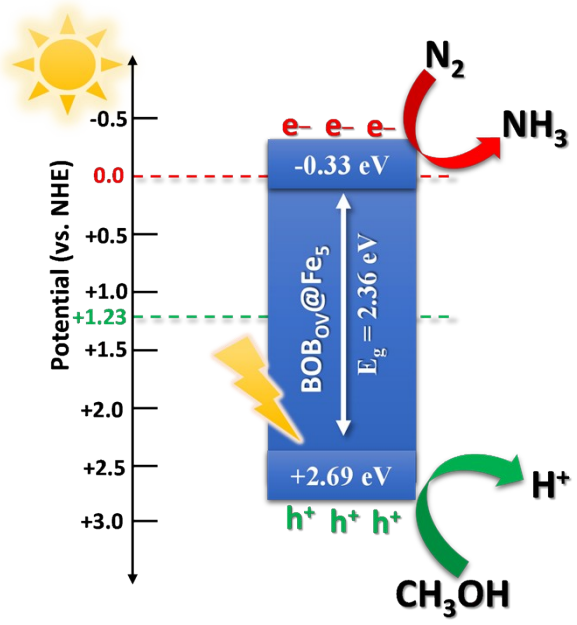

Figure S13. Schematic presentation of photocatalytic N_2 reduction through $BOB_{OV}@Fe_5$.

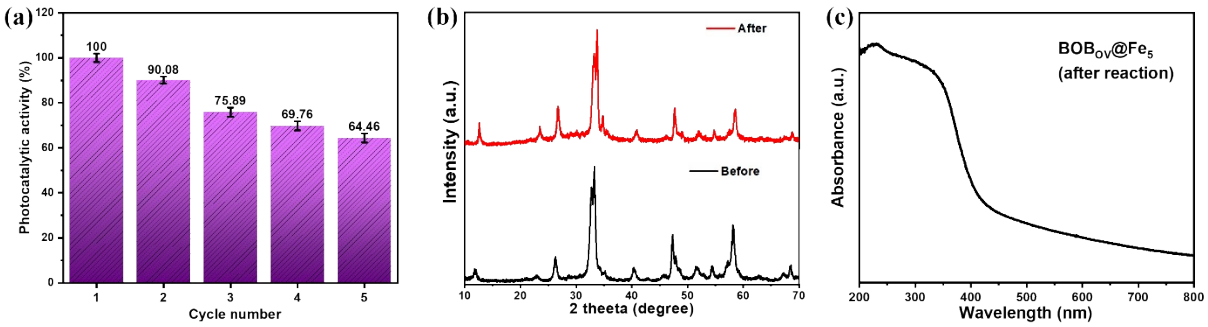

Figure S14. (a) Cyclic stability tests, (b) XRD pattern before and after the stability study, (c) UV-vis DRS absorbance spectra of the used photocatalyst.

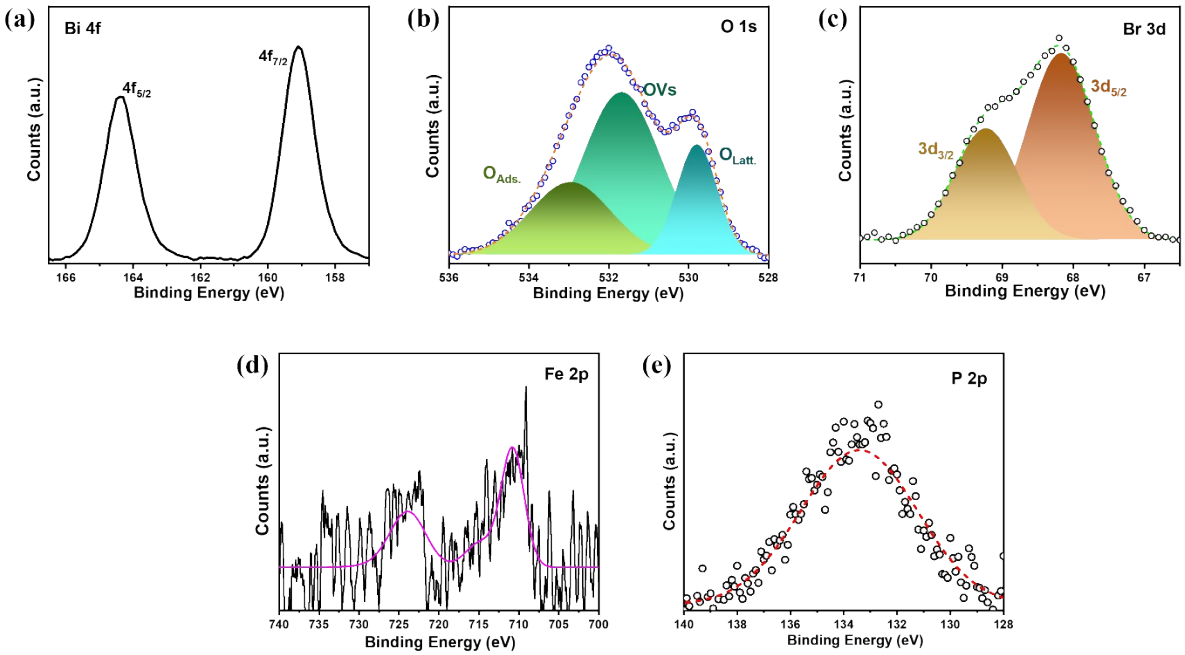

Figure S15. High-resolution XPS spectra of Bi 4f, O 1s, Br 3d, Fe 2p, and P 2p of the used photocatalyst - BOB$_{OV}$@Fe$_5$.

Table S1. Comparative areal percentages of deconvoluted peaks of O 1s XPS of the photocatalyst, before and after the stability study.

	O$_{Latt.}$(%)	**OVs (%)**	**O$_{Ads.}$(%)**
Before	22.09	57.76	20.15
After	19.47	50.65	25.47

Table S2. Comparison table for photocatalytic NH_3 production with other reports with respect to this work.

S. No.	Photocatalyst	Solution	NH_3 production rate	Light Source	Refs.
1	Bi_2WO_6	5% MeOH	320.2 μmol $L^{-1}h^{-1}$	300 W Xe lamp	17
	g-C_3N_4		131.3 μmol $L^{-1}h^{-1}$		
	Bi_2WO_6/g-C_3N_4		697.2 μmol $L^{-1}h^{-1}$		
2	BiOBr	Water	20.15 μmol $g^{-1}h^{-1}$	300 W Xe lamp	18
	$Bi_4O_5Br_2$		11.43 μmol $g^{-1}h^{-1}$		
	BiOBr/$Bi_4O_5Br_2$		66.87 μmol $g^{-1}h^{-1}$		
3	$CdWO_4$	0.5% MeOH	87.9 μmol $g^{-1}h^{-1}$	300 W Xe ($\lambda \geq 400$ nm)	19
	$Bi_4O_5Br_2$		162.0 μmol $g^{-1}h^{-1}$		
	$CdWO_4$/$Bi_4O_5Br_2$		501.0 μmol $g^{-1}h^{-1}$		
4	Bi_2MoO_6	Water	3 μmol $L^{-1}h^{-1}$	45 W LED Bulb	2
	Bi_2WO_6		1 μmol $L^{-1}h^{-1}$		
	$BMWO_{0.4}$		320.2 μmol $L^{-1}h^{-1}$		
5	PANI/$ZnIn_2S_4$	20% MeOH	290 μmol $L^{-1}h^{-1}$	Visible Light ($\lambda \geq 420$ nm)	20
6	C_3N_4/r-Ti_3C_2-2	20% MeOH	328.9 μmol $L^{-1}h^{-1}$	300 W Xe lamp ($\lambda \geq 420$ nm)	21
7	BiOBr	Water	4.8 μmol $g^{-1}h^{-1}$	Xe lamp ($\lambda \geq 420$ nm)	22
	Ti_3C_2		4.47 μmol $g^{-1}h^{-1}$		
	BiOBr/Ti_3C_2		234.6 μmol $g^{-1}h^{-1}$		
8	BOB	1% MeOH	67.5 μmol $g^{-1}h^{-1}$	White LED	This study
	BOB_{OV}		105 μmol $g^{-1}h^{-1}$		
	BOB_{OV}@Fe_5		385.5 μmol $g^{-1}h^{-1}$		

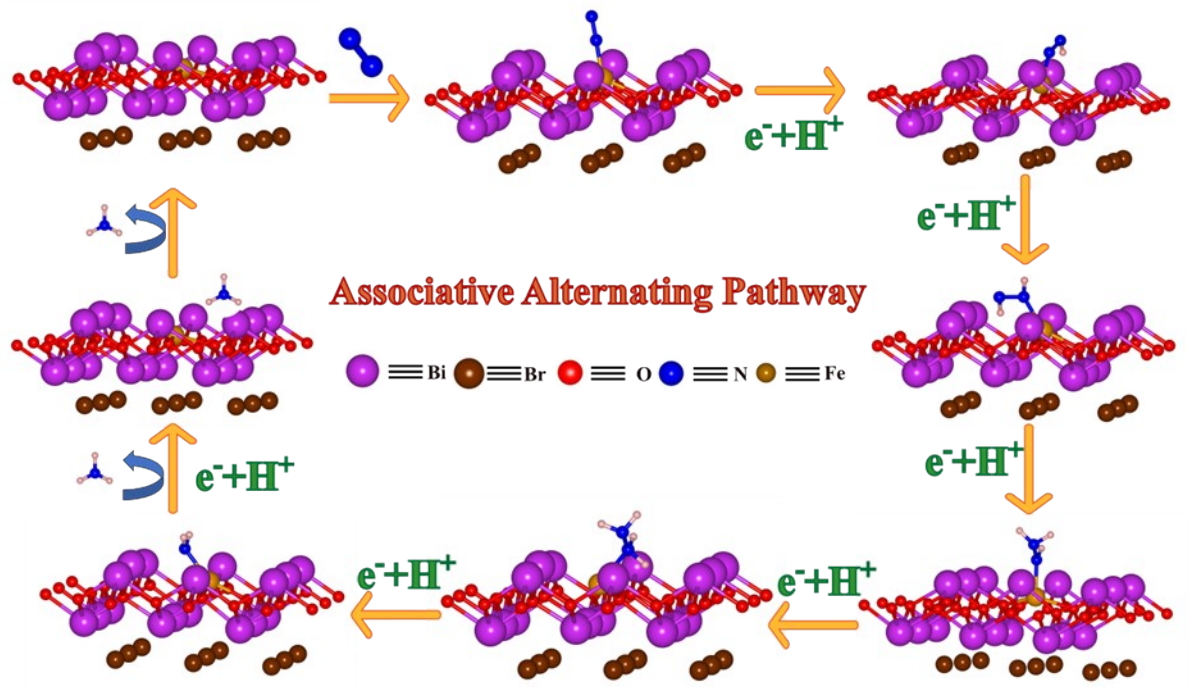

Figure S16. Equilibrium structures of reaction intermediates involved in the associative alternating pathway of NRR on the surfaces of the $BOB_{OV}@Fe_x$.

References:

1 A. Kumar, M. Kumar, V. Navakoteswara Rao, M. V. Shankar, S. Bhattacharya and V. Krishnan, *J Mater Chem A Mater*, 2021, **9**, 17006–17018.

2 M. Sharma, A. Kumar, D. Gill, S. Jaiswal, A. Patra, S. Bhattacharya and V. Krishnan, *ACS Appl Mater Interfaces*, 2023, **15**, 55765–55778.

3 Y. Zhang, S. Gu, X. Zhou, K. Gao, K. Sun, D. Wu, J. Xia and X. Wang, *Catal Sci Technol*, 2021, **11**, 4783–4792.

4 C. Zhang, G. Chen, C. Lv, Y. Yao, Y. Xu, X. Jin and Q. Meng, *ACS Sustain Chem Eng*, 2018, **6**, 11190–11195.

5 X. Xue, R. Chen, H. Chen, Y. Hu, Q. Ding, Z. Liu, L. Ma, G. Zhu, W. Zhang, Q. Yu, J. Liu, J. Ma and Z. Jin, *Nano Lett*, 2018, **18**, 7372–7377.

6 Y. Yu, P. Zhang, R. Tuerhong, K. Chai, X. Du, X. Su, L. Zhao and L. Han, *Sep Purif Technol*, 2025, **364**, 132501.

7 G. Kresse and J. Hafner, *Phys Rev B*, 1993, **47**, 558.

8 G. Kresse and J. Furthmüller, *Phys Rev B*, 1996, **54**, 11169.

9 G. Kresse and D. Joubert, *Phys Rev B*, 1999, **59**, 1758.

10 M. Ernzerhof and G. E. Scuseria, *J Chem Phys*, 1999, **110**, 5029–5036.

11 A. Erba, J. K. Desmarais, S. Casassa, B. Civalleri, L. Donà, I. J. Bush, B. Searle, L. Maschio, L. Edith-Daga, A. Cossard, C. Ribaldone, E. Ascrizzi, N. L. Marana, J. P. Flament and B. Kirtman, *J Chem Theory Comput*, 2023, **19**, 6891–6932.

12 J. Muscat, A. Wander and N. M. Harrison, *Chem Phys Lett*, 2001, **342**, 397–401.

13 S. Grimme, J. Antony, S. Ehrlich and H. Krieg, *Journal of Chemical Physics*, 2010, **132**, 154104.

14 M. F. Peintinger, D. V. Oliveira and T. Bredow, *J Comput Chem*, 2013, **34**, 451–459.

15 K. Momma and F. Izumi, *urn:issn:0021-8898*, 2011, **44**, 1272–1276.

16 H. Joshi, N. Sinha, K. Parveen and S. Pakhira, *Energy and Fuels*, 2023, **37**, 19771–19784.

17 E. Dhanaraman, A. Verma, P. H. Chen, N. Di Chen, Y. Siddiqui and Y. P. Fu, *Solar RRL*, 2024, **8**, 2300981.

18 H. Wang, Z. Chen, Y. Shang, C. Lv, X. Zhang, F. Li, Q. Huang, X. Liu, W. Liu, L. Zhao, L. Ye, H. Xie and X. Jin, *ACS Catalysis* , 2024, **14**, 5779–5787.

19 C. Zhao, X. Li, L. Yue, X. Ren, S. Yuan, Z. Zeng, X. Hu, Y. Wu and Y. He, *ACS Appl Nano Mater*, 2023, **6**, 15709–15720.

20 S. Chen, F. Xie, X. Wang, X. Zhao and Z. Tang, *New Journal of Chemistry*, 2020, **44**, 7350–7356.

21 B. Chang, Y. Guo, H. Liu, L. Li and B. Yang, *J Mater Chem A Mater*, 2022, **10**, 3134–3145.

22 Y. Fang, Y. Cao, B. Tan and Q. Chen, *ACS Appl Mater Interfaces*, 2021, **13**, 42624–42634.